ACS Catalysis

pubs.acs.org/acscatalysis

Research Article

Elucidation of the Hydrogen Evolution Reaction on a Photochemical Molecular Device

Miftahussurur Hamidi Putra, Alexander K. Mengele, Benedikt Bagemihl, Sven Rau, Michael Busch, and Axel Groß*

Cite This: https://doi.org/10.1021/acscatal.6c03235

Read Online

ACCESS | Metrics & More | Article Recommendations | Supporting Information

ABSTRACT: The direct conversion of solar energy to produce useful chemical products such as molecular hydrogen is one of the ultimate goals of photocatalysis. Photochemical molecular devices enable such a process cost-efficiently while offering additional benefits like repairability. We present here a full mechanism for the complete photo-induced catalytic hydrogen evolution reaction by combining a Ru-containing photocenter and a Pt-based catalytically active center in one molecular device. State-of-the-art quantum-chemical calculations shed light on the interplay between light-driven electron transfer processes and activation of protons as substrates. They reveal an induction process and the crucial role of the formation of unpaired electronic states corresponding to a doublet and subsequent higher spin multiplicities. Furthermore, the study indicates that sacrificial donors not only provide electrons but also act as a proton regulator in combination with the bridging ligand acting as a base. Based on the mechanistic understanding derived from the detailed atomistic calculations, our study provides design principles for operative photochemical molecular devices. Thus, our results that are validated through the comparison with experimental spectroscopic data are expected to alter the perspective on elementary concepts of artificial photosynthesis.

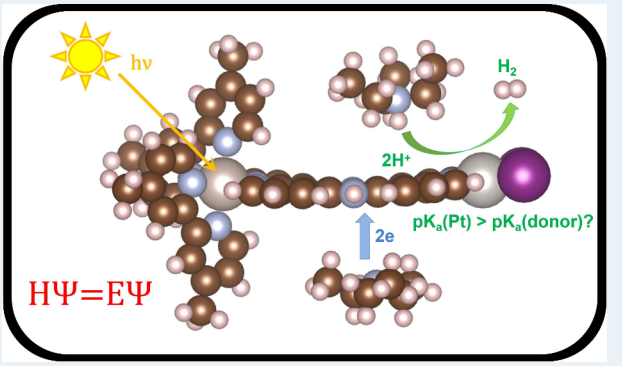

KEYWORDS: *photocatalyst, hydrogen evolution reaction, density functional theory, homogeneous catalysis, catalytic cycle, photochemical molecular device*

INTRODUCTION

In this work, we present a quantum chemical study of the photo-induced hydrogen evolution reaction on a photochemical molecular device (PMD) that combines a Ru-containing photocenter and a Pt-based catalytic center. Green H_2 is regarded as an important energy carrier for the necessary transformation toward more sustainable energy technologies.[1−4] However, the efficient and sustainable production of molecular hydrogen still represents a severe challenge. Ideally, the energy of sunlight is directly used to catalyze the hydrogen evolution reaction (HER). Traditionally, this is achieved by using separate photovoltaic devices and HER electrocatalysts. On the other hand, there is a growing interest in artificial photosynthesis,[5] which is inspired by the impressive molecular machinery of natural photosynthesis, such as photosystem I,[6] as illustrated in the upper panel of Figure 1. Photosystem I corresponds to a large protein complex that mediates light-induced electron transfer to ferredoxin, which then acts as a reducing agent for various processes, including NADPH formation. However, Figure 1 indicates that natural photosynthesis is based on a sequence of complicated reactions. Furthermore, it is optimized by evolution to sustain the living cell and therefore operates with low efficiency in terms of harvestable chemical energy.

Inspired by the growing understanding of biological photosynthesis, artificial photosynthesis based on photochemical molecular devices integrating a photoredox active photosensitizer and catalyst units linked by a bridging ligand[9] represents a promising alternative for the production of green hydrogen. This has motivated intensive research efforts aiming at a better understanding and the improvement of photocatalytic processes.[12−22] There has been a rapid development of a plethora of PMDs illustrated in Figure 1. PMDs have been developed that can surpass thermal molecular catalysis (Figure 1a[7]) and have then been further tailored by suitable ligand substitution

Received: April 24, 2026
Revised: September 13, 2026
Accepted: September 14, 2026

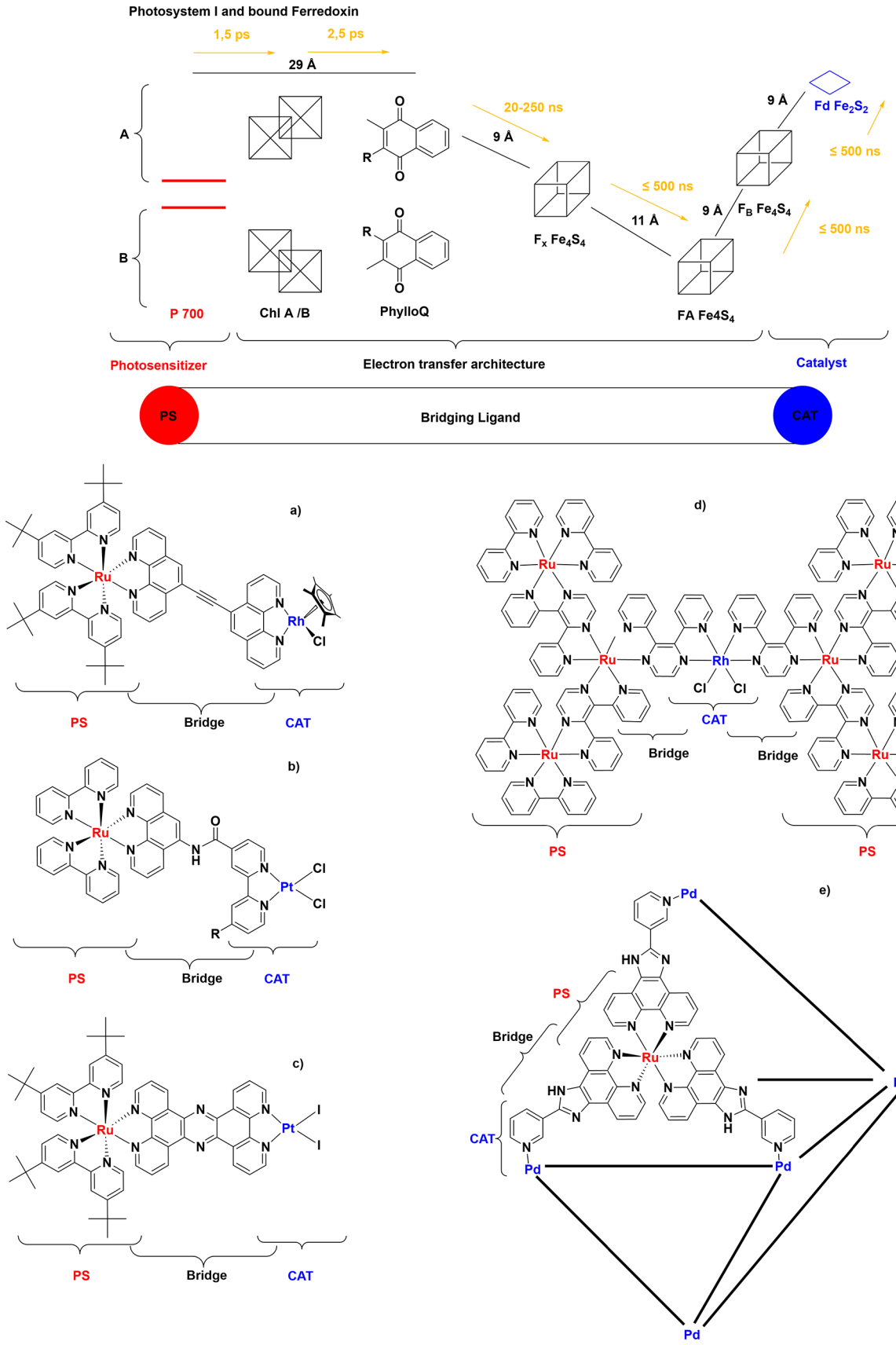

Figure 1. continued

https://doi.org/10.1021/acscatal.6c03235
ACS Catal. XXXX, XXX, XXX–XXX

Figure 1. Comparison of photosystem I[6] (upper panel) with examples of different photochemical molecular devices consisting of a photoredox active photosensitizer (PS) and a catalyst (CAT) unit linked by a bridging ligand (overall charges are omitted for clarity): (a) a photochemical molecular device (PMD) surpassing thermal molecular catalysis,[7] (b) PMDs with designed catalytic activity by ligand substitution,[8] (c) PMD with active repair capacity,[9] (d) heptametallic PMD with light-harvesting chromophore architecture,[10] and (e) material-integrated PMD.[11] Chemical structural formulas have been created based on the information given in the respective references.

(Figure 1b[8]). The photocatalytic hydrogen formation of a damaged PMD can be restored by applying active repair mechanisms (Figure 1c[9]). PMDs with several light-harvesting chromophores improving their performance have been successfully designed (Figure 1d[10]). It has already been accomplished to integrate hydrogen-evolving PMDs into materials. However, the incorporation of several light-harvesting and catalytic active centers that provide multiple energy transfer and electron collection pathways (Figure 1e[11]) has so far hampered a detailed mechanistic understanding.

However, it is clear that an accelerated rational development and optimization of catalysts requires a thorough understanding of the mechanistic details of the particular reaction to be catalyzed. It is fair to say that a detailed mechanistic understanding of a complete molecular photocatalytic reaction cycle is conspicuously absent from the literature. This is, to a certain extent, rather surprising considering that, first, many experimental studies have already addressed the relatively simple electrocatalytic HER reaction involving just two protons and two electrons, which even led to the coinage of Tafel, Heyrovsky, and Volmer step terminology in electrocatalysis.[23,24] Additionally, the photoelectrocatalytic HER is also relatively well understood.[9,25−28] Nonetheless, the mechanistic details of the photocatalytic HER remain elusive to a large extent. Furthermore, it is also important to realize that the photocatalytic HER involves additional complexity compared to the electrocatalytic HER arising from excited-state processes, including photoexcitation, charge separation, and excited-state dynamics, which are absent in conventional electrocatalytic pathways. Spectroscopic investigations are often limited to the initial one-electron transfer steps, and measurements under operando conditions are difficult to implement. In addition, the identification of critical intermediates is typically hindered by the fact that they lack suitable spectroscopic signatures, in particular if photochemically inactive co-substrates like the electron donors are involved.

The whole field of artificial photosynthesis for catalytic formation of multielectron products such as hydrogen molecules obviously requires a more thorough understanding of the catalytic process. Above, we described the accelerated development of understanding of the catalytic steps in biological photosynthesis enabled by a detailed analysis using theoretical methods. Similarly, the current situation in artificial photosynthesis research calls for theoretical support by quantum-chemical calculations.[29] However, to the best of our knowledge, up to now, only a few studies have, in fact, explored the mechanistic aspects of the photo-induced hydrogen evolution, mainly in Pt-based molecular catalysts,[8,30] but also for Ru complexes.[31] These previous theoretical investigations typically did not consider the full photochemical molecular device but were rather limited to just the catalytic unit.

Here, we present a complete catalytic cycle of the photo-induced HER on a photochemical molecular device by combining the mechanistic details of all reaction steps with the corresponding electronic transitions. This cycle has been derived using a quantum-chemical approach closely coupled with experiments, thus validating the calculations. Our DFT calculations confirm the existence of an experimentally clearly identified induction process,[32] which is necessary to activate the photochemical molecular device and essentially represents a light-induced reduction coupled with protonation of the bridging ligand. The so-formed radical state located on the bridging ligand is a persistent entity during the whole catalytic cycle; in other words, subsequent steps in the mechanism involve this doublet ground state as the actual catalyst. The important catalytic role of such unsaturated or radical states has also already been identified for metal-oxide catalysts.[33] Furthermore, we reveal the important role of the protonation of the photomolecular device for its stability during the hydrogen evolution reaction. Thus, we provide design rules for active molecular photocatalysts.

In detail, we have employed density functional theory (DFT) to elucidate the complete cycle of the photocatalytic hydrogen evolution reaction, which, to the best of our knowledge, has not been achieved before. The electrochemical environment has been taken into account using an implicit solvent model. In addition, time-dependent density functional theory (TD-DFT) has been utilized to comprehensively analyze the excitation properties of the intermediates during the photocatalytic process. This allows us to validate the identified reaction intermediates by comparing their spectroscopic signatures with the wealth of experimental information. To showcase this approach, we have chosen $[(tbbpy)_2Ru(tpphz)PtI_2]^{2+}$ (tbbpy = 4,4′-di-*tert*-butyl-2,2′-bipyridine, tpphz = tetrapyrido [3,2-a:2′,3′-c:3‴-h:2‴,3‴-j] phenazine) or simply $RuPtI_2$ as the photochemical molecular device, which has shown great promise for the photocatalytic hydrogen evolution.[9,16,34] Very relevant to this study are the high chemical stability of the PtI_2 center bound to the NN-chelating extended π system of the bridging ligand, tpphz.[34] It has been demonstrated that the synergy between the extended π-system of tpphz and the specific bonding at the square planar PtI_2 sphere is crucial for this high stability during the catalytic cycle.

By following this approach, we not only gain unprecedented insights into the mechanism of hydrogen evolution from $RuPtI_2$ but also elucidate how this photocatalyst molecule protects itself from degradation. Identifying the complete photocatalytic HER cycle is invaluable for future advancements in developing photochemical molecular devices to achieve optimal hydrogen production. However, we like to add a note of caution. In this paper, we present a plausible complete catalytic cycle of the photo-induced HER. Yet, it is important to note that not all reaction intermediates are necessarily observable by experiments as they are often too short-lived to provide a signal detectable by experiments. Furthermore, considering the turnover numbers per complex derived from experiments, such as reported in ref 9, shows that a successful photocatalytic reaction corresponds to an extremely rare event on the microscopic scale, on the order of one event every several minutes. This also

https://doi.org/10.1021/acscatal.6c03235
ACS Catal. XXXX, XXX, XXX−XXX

means that the reaction steps proposed in our theoretical study occur rather infrequently, and our proposed reaction mechanism corresponds to a rare event. However, our reaction mechanism is consistent with all experimental observations, as described in detail below; therefore, we are very confident that our study provides a rather realistic possible scheme for the photocatalytic HER cycle.

COMPUTATIONAL DETAILS

In this work, we investigate the potential intermediates involved in the photocatalytic HER of $RuPtI_2$ using DFT calculations. We started our investigation by scanning the possible configuration of the $RuPtI_2$ photocatalyst under reaction conditions. Our calculations also include the careful analysis of different charge and spin states. All DFT calculations were performed using the Gaussian 16 Rev C.01 code.[35] The B3LYP functional,[36,37] together with Grimme DFT-D3 dispersion corrections and Becke-Johnson damping,[38] in combination with a def2-SVP basis set,[39,40] has been employed for the geometry optimization. Afterward, single-point calculations at the relaxed geometries using the same functional but a larger def2-TZVP basis set[39,40] have been performed to obtain converged energies on the single-particle level. Basis set superposition errors (BSSE)[41] at the def2-TZVP level were estimated to be small (approximately 0.05 eV).[42,43] Since all energetic comparisons in this work are based on relative energies between transition states and their preceding intermediates along a common reaction coordinate, the residual error is expected to largely cancel.

In the search for the most favorable reaction path, we have been guided by the Brønsted–Evans–Polanyi principle,[44] which states that there is a close relation between the height of activation barriers and the reaction energy, i.e., we have considered the reaction path with the energetically most favorable intermediates. Transition states between these intermediates were confirmed by the presence of a single imaginary mode along the reaction coordinate. Depending on the nature of the transition state, only an implicit or a simplified micro-solvation model combined with an implicit solvation model was used. Thus, the barriers correspond to a worst-case scenario and the true barriers may be lower due to beneficial interactions with the solvent.

The theoretical modeling of photocatalytic and electrocatalytic processes requires an appropriate consideration of the interface between the catalyst and the electrolyte.[45] In the experiments, a 6:3:1 (v/v) mixture of acetonitrile, triethylamine, and water was used as the solvent, with a final catalyst concentration of 70 μM in the catalytic solution. Subsequently, the solution was irradiated using four LED arrays (470 nm, 30–40 mW cm^{-2}) and continuously air-cooled to maintain the temperature at 22 °C. To account for the solvent environment in the theoretical calculations, an explicit description of the full solvent mixture would in principle be desirable. However, quantum chemical calculations of extended solvated complexes using explicit solvent models remain computationally prohibitive. Therefore, we employed an implicit solvation model based on the solvation model density (SMD) approach.[46] Such implicit solvent models cannot capture specific solvent organization or the preferential ordering of co-solvents at the molecular level.[47] In the present calculations, we therefore used an implicit solvent with the dielectric constant of acetonitrile. This choice is motivated by experimental observations showing that the addition of triethylamine (NEt_3) and water to acetonitrile does not significantly affect the optical properties of the $RuPtI_2$ complex.[9] Furthermore, no substitution reactions in $RuPtI_2$ have been experimentally observed under these conditions, which allows the simplifications implemented throughout this study for this specific complex.[9] Furthermore, TD-DFT[48,49] has been utilized to comprehensively analyze the excitation properties of the intermediates during the photocatalytic process. For the TD-DFT calculations, we employed the same setup as used in the geometry optimization.

The selection of the B3LYP-D3(BJ) functional in this study was based on several considerations. First of all, previous computational studies have demonstrated that DFT methods, including B3LYP-based approaches, can provide reasonable estimates of the relative energy differences between high-spin and low-spin states in transition-metal complexes, although with an intrinsic uncertainty associated with the choice of functional.[50] Therefore, it might well be that the relative quantitative ordering of the spin states can be functional-dependent and should therefore be considered qualitatively rather than quantitatively. Furthermore, in our previous work[16] summarized in Section 4 of the Supplementary Information, we systematically benchmarked B3LYP-D3(BJ) against a range of functionals, including global hybrid functionals (PBE0), range-separated hybrid functionals (CAM-B3LYP, HSE06), and a meta-hybrid functional (M06, M06-2X). In that study, B3LYP-D3(BJ) showed the best overall agreement with the experimental UV–vis spectra. Furthermore, proton solvation energies calculated using the same level of theory were found to be in good agreement with experimental reference values,[51] providing additional support for the suitability of this functional in describing thermochemical trends relevant to the present system.

To assess the probability of proton binding to the photochemical molecular device, we derived values of the acid dissociation constant pK_a from the calculated proton solvation energies using the isodesmic method with an accuracy of around 1.5 pK_a in water.[51−57] Based on our calculations, the proton solvation energy value in acetonitrile is −11.20 eV, which compares well with previously measured and calculated values.[58,59] For details of the method for calculating the proton solvation energy and pK_a, we refer to the Supplementary Information (SI) and the literature.[51,60] The reduction energy of $RuPtI_2$ is determined from DFT calculations using the NEt_3/NEt_3^+ redox couple as the reference. Finally, to examine the changes in the electronic distribution of $RuPtI_2$ throughout the reaction pathway, Mulliken charge analysis[61] was performed. Although Mulliken charges are known to exhibit a dependence on the choice of basis set, they remain useful for qualitatively describing relative changes in the electron distribution.[62−64] Therefore, in this work, we focus on the charge differences rather than the absolute charge values to characterize the electronic distribution changes associated with the reaction intermediates.

RESULTS AND DISCUSSION

In this study, we consider the $RuPtI_2$ complex, which consists of a Ru polypyridyl unit that acts as a photosensitizer and a PtI_2 catalyst. Both units are connected by a tpphz bridge.[9,34] Previous measurements showed remarkable HER activity for this complex. A turnover number (TON) exceeding 450 was observed in mixtures of acetonitrile (MeCN), water, and triethylamine (NEt_3) in a volumetric composition of 6:1:3,[9]

https://doi.org/10.1021/acscatal.6c03235
ACS Catal. XXXX, XXX, XXX−XXX

with NEt_3 acting as a sacrificial electron donor. To the best of our knowledge, this result represents one of the highest photocatalytic hydrogen gas production yields among photochemical molecular devices utilizing platinum-based catalysts. In addition, $RuPtI_2$ exhibits not only high photocatalytic performance but also good stability as a catalyst under operational conditions.[9,19,34] Beyond its high stability, $RuPtI_2$ can be repaired by different pathways, which reinvigorate its photocatalytic capacity.[9,32] This very rare capability renders a detailed understanding of its actual photocatalytic mechanism very important.

Before considering the explicit calculations, we like to first recall the basics of the electrocatalytic HER, as photo- and electrochemistry likely share many mechanistic similarities. The first step in the HER typically consists of the Volmer step:[65]

$$\text{Volmer}: \ \text{Cat} + \text{H}^+ + \text{e}^- \rightarrow \text{Cat} - \text{H} \qquad (1)$$

which corresponds to the reductive adsorption of a proton from the electrolyte on the active site of the catalyst denoted by ∗. To complete the HER, there are two possible mechanisms, either the Volmer–Tafel mechanism involving a chemical recombination reaction or the Volmer–Heyrovsky mechanism involving a second charge-transfer step:[65−73]

$$\text{Tafel}: \ 2\text{Cat} - \text{H} \rightarrow 2\text{Cat} + \text{H}_2 \qquad (2a)$$

$$\text{Heyrovsky}: \ \text{Cat} - \text{H} + \text{H}^+ + \text{e}^- \rightarrow \text{Cat} + \text{H}_2 \qquad (2b)$$

The PMD considered in our study contains only one catalytic center, which means that it is very unlikely that the Tafel mechanism requiring two adsorbed hydrogen atoms can be operative. However, as illustrated in the Volmer–Tafel (eqs 1 and 2a) and the Volmer–Heyrovsky (eqs 1 and 2b) mechanisms, the electrocatalytic HER requires the transfer of two electrons to the two protons. These electrons have to be provided by the flowing current to the electrocatalyst. Molecular photocatalysis is related to the electrocatalysis if viewed from the perspective of the individual mechanistic steps taking place at the catalysis center, describing the ground-state chemistry occuring there. It is fundamentally different from the perspective of the source and supply of the required electrons. They are provided by consecutive one-electron transfer steps from the PS to the CAT center, which can only take place if a (sacrificial) electron donor is oxidized. Without irradiation, the $RuPtI_2$ complex is inactive with respect to the HER. Thus, the catalytic activity of the $RuPtI_2$ complex has to be initiated by the photoinduced electron transfer from the photoactive Ru center of the complex to its PtI_2 catalyst. These transfer steps must then be coupled to oxidation of the electron donor, which commonly is triethylamine (TEA or NEt_3) for this photocatalytic system. Thus, our quest for the elucidation of the microscopic steps in the photo-induced HER of the $RuPtI_2$ complex was performed as a search for possible electron- and proton-transfer steps guided by experimental spectroscopic information where available.[9,25−27,34]

NEt_3 serves as a reductive quencher for the charge-separated state in $RuPtI_2$, reducing the photochemically formed transient Ru(III) to the Ru(II) state. This leads to the formation of NEt_3 radical species, which do show a complicated reaction network involving proton transfer or even hydrogen atom transfer steps, which are highly dependent on specific reaction conditions.[74] More detailed, very recent investigations using pulse radiolysis methods have highlighted the reducing power of the radical intermediates, which may play a role in light-driven catalytic reactions as presented here.[75] Experimental investigations for $RuPtI_2$ using different sacrificial electron donors like BNAH or BIH do show significant photocatalytic H_2 formation reactions, surpassing the catalytic results obtained for NEt_3.[76] The role of the NEt_3 radical species in the photocatalysis with $RuPtI_2$ has to be investigated in more detail, but it seems to play a less pronounced role than in intermolecular photochemical electron transfer pathways.[77]

With respect to the chemical environment, in which the $RuPtI_2$ complex is dissolved, challenges not only arise from the unknown solvent properties of the acetonitrile, water, and NEt_3 mixture but are also caused by the unknown pH value of electrolytes under catalytic conditions. Therefore, we first discuss the calculated pK_a values of the three protonated species H_3O^+, NEt_3H^+, and $MeCNH^+$ in acetonitrile. Note that the value of the acid dissociation constant pK_a is directly proportional to the standard Gibbs free energy change for the proton transfer reaction. Our DFT calculations reveal that H_3O^+ and $MeCNH^+$ have low pK_a values of −7.2 and −2.2, respectively. Water can also be excluded as a proton donor since earlier studies indicate that its pK_a in acetonitrile rises, owing to the poor stabilization of OH^-, to 40.[51,53] As a result, water and acetonitrile are predominantly not protonated under reaction conditions. In contrast, NEt_3H^+ displays a pK_a of 17.6, which is satisfactorily close to the experimental value of 18.8.[78] Consequently, for the HER on $RuPtI_2$ to occur, the pK_a value of the metal hydride at $RuPtI_2$ must be higher than 17.6; otherwise, the protons would hardly bind to the photocatalyst. Based on this requirement, we computationally explored a multitude of reasonable reaction pathways for the light-driven HER at $RuPtI_2$.

The complete proposed catalytic cycle of the light-driven HER on $RuPtI_2$ is depicted in Scheme 1. In its electronic ground state, $RuPtI_2$ is inactive toward the HER as it has a highly acidic pK_a of −4.7 on the PtI_2 catalyst. The nitrogen atoms on the bridging ligand represent additional possible protonation sites. However, they also have low pK_a values of 3.2 and −4.4 for the first and second protonation on the bridge, respectively; therefore, no protons are bound to $RuPtI_2$ in its electronic ground state.

The HER is initiated by the reductive activation of $RuPtI_2$ through the initial electronic excitation to state **1***, requiring an energy of ca. 2.85 eV (λ = 435 nm, S17, see Scheme 2). This excitation corresponds to a singlet metal-to-ligand charge transfer (^{1}MLCT) involving electron transfer from the ruthenium metal center to the ligands (see Figure 2a). Afterward, the excitation process is followed by an intersystem crossing (ISC) and vibrational relaxation to form intermediate **2**. This intermediate differs only in the spin state and electron distribution from intermediate **1**. It corresponds to a ^{3}MLCT state with excess electron density at the tpphz ligand. In the MLCT, approximately 0.7e are shifted from the photosensitizer (ruthenium and bipyridine ligand) to the tpphz bridge (see Mulliken charge and spin state shown in Figures S1 and S2). As the next step, the sacrificial electron donor triethylamine (NEt_3) donates an electron to intermediate **2**, as experimentally well-known,[79−83] with ΔG = −0.22 eV, and thus reduces the

https://doi.org/10.1021/acscatal.6c03235
ACS Catal. XXXX, XXX, XXX−XXX

Scheme 1. Overall Reaction Mechanism of Light-Driven Hydrogen Evolution Reaction with $RuPtI_2$[a]

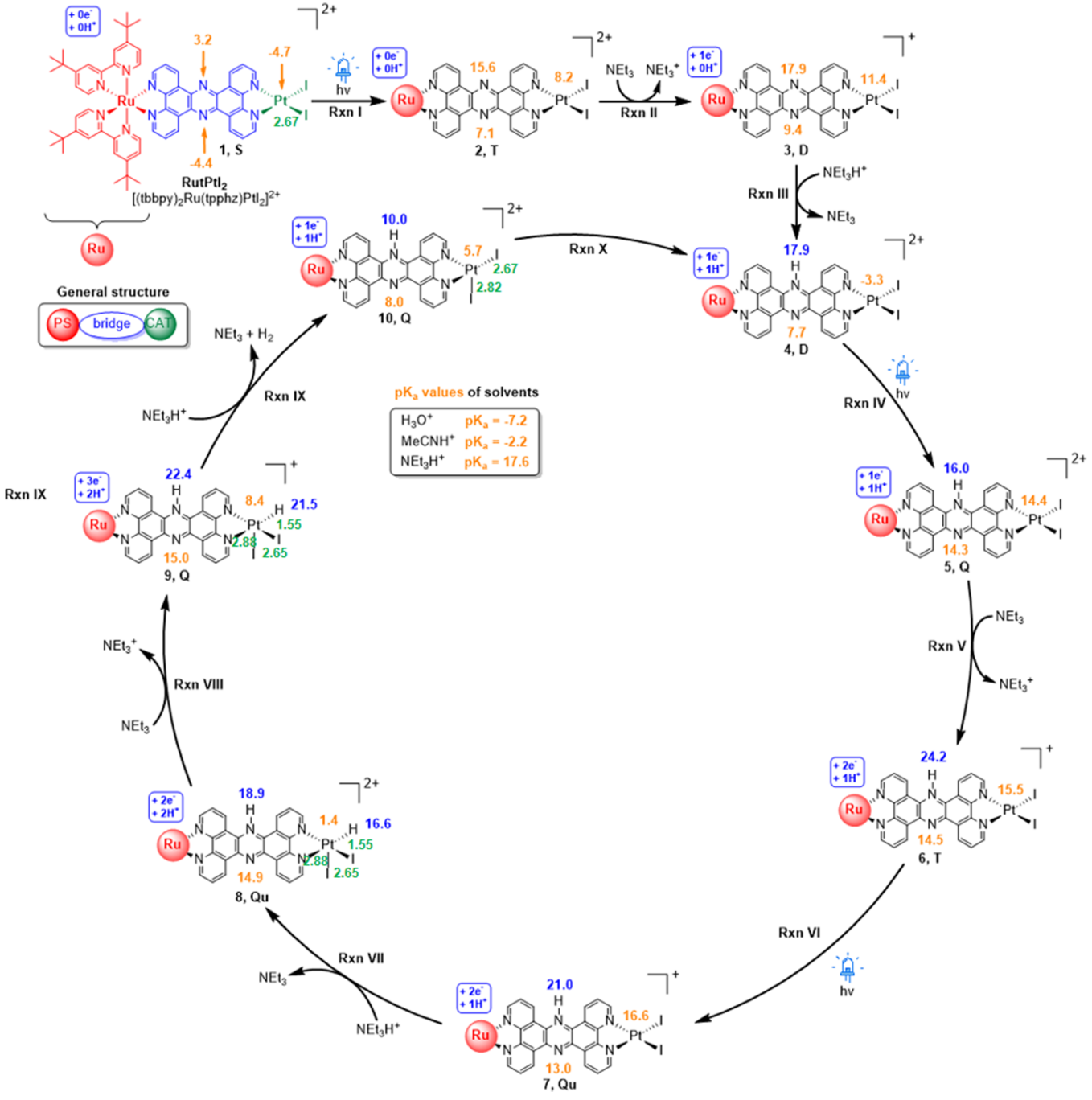

[a]Numeric labeling of intermediates along with their spin states (S = singlet, D = doublet, T = triplet, Q = quartet, Qu = quintet) is given in black below each species. pK_a values of the N and Pt sites of the respective intermediates are given in orange color, whereas the pK_a values of the deprotonation of already occupied hydrogen sites are printed in blue. The Pt–I and Pt–H bond lengths are printed in green and represented in Angstrom (Å). The total number of electrons and protons stored at $RuPtI_2$ is given in blue boxes. Abbreviations: photosensitizer (PS), catalyst unit (CAT). Top left: Molecular structure of $RuPtI_2$ and general design concept for intramolecularly operating photocatalysts.

photocatalytic molecule to produce intermediate **3**, as shown in Rxn II, where the excess electron is accumulated at the bridge (see Figures S1 and S2). The probability of Pt–H bond formation in intermediates **2** and **3** is very low due to their pK_a values being approximately 9 and 6 units, respectively, lower than that of NEt_3H^+. Therefore, both intermediates cannot be considered as active species in the photocatalytic process.

However, one of the nitrogen atoms in the bridging ligand of intermediate **3** possesses a pK_a of 17.9, which is larger than the pK_a of NEt_3H^+. Consequently, the proton transfer from

https://doi.org/10.1021/acscatal.6c03235
ACS Catal. XXXX, XXX, XXX–XXX

Scheme 2. Reaction Energetics along the Catalytic Cycle Shown in Scheme 1a

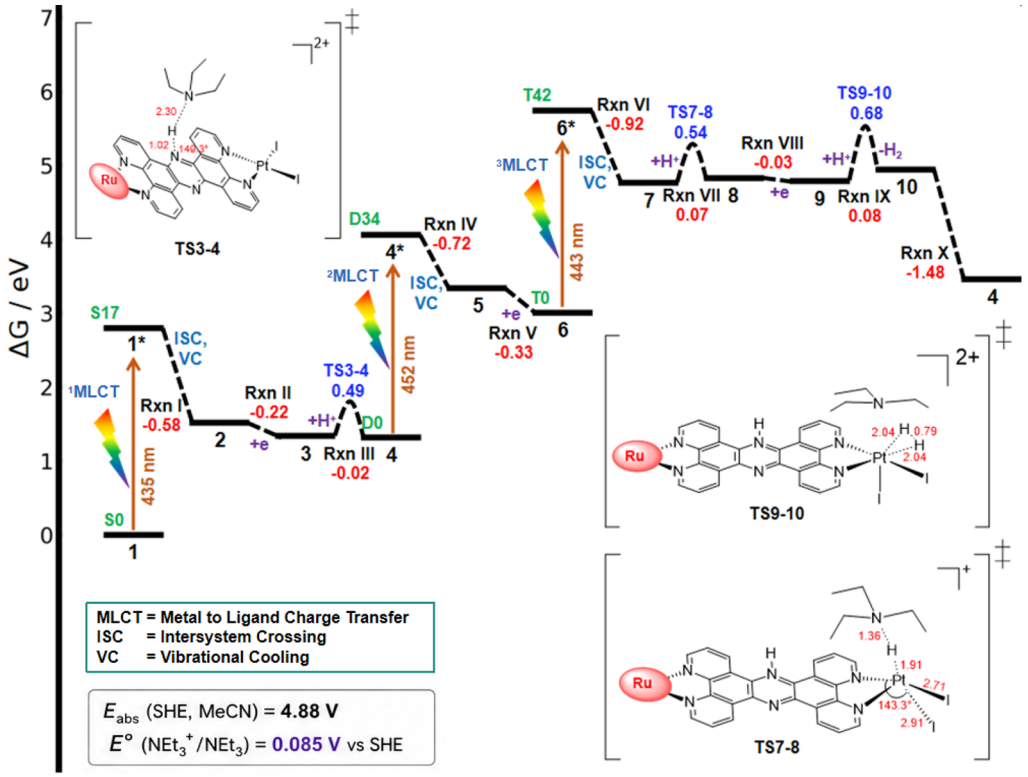

[a]The reaction energies are shown in red color, the activation energies of selected steps are printed in blue, and all energies are given in eV. Here, NEt_3H^+ is considered as the proton source. In addition, the structure of the three major transition states is illustrated with the bipyridine ligands being removed for the sake of clarity. The redox potentials are converted to the SHE scale using the computed $NEt_3^{\bullet+}/NEt_3$ redox potential of 0.085 V vs SHE (with an absolute SHE potential of 4.88 V in MeCN).

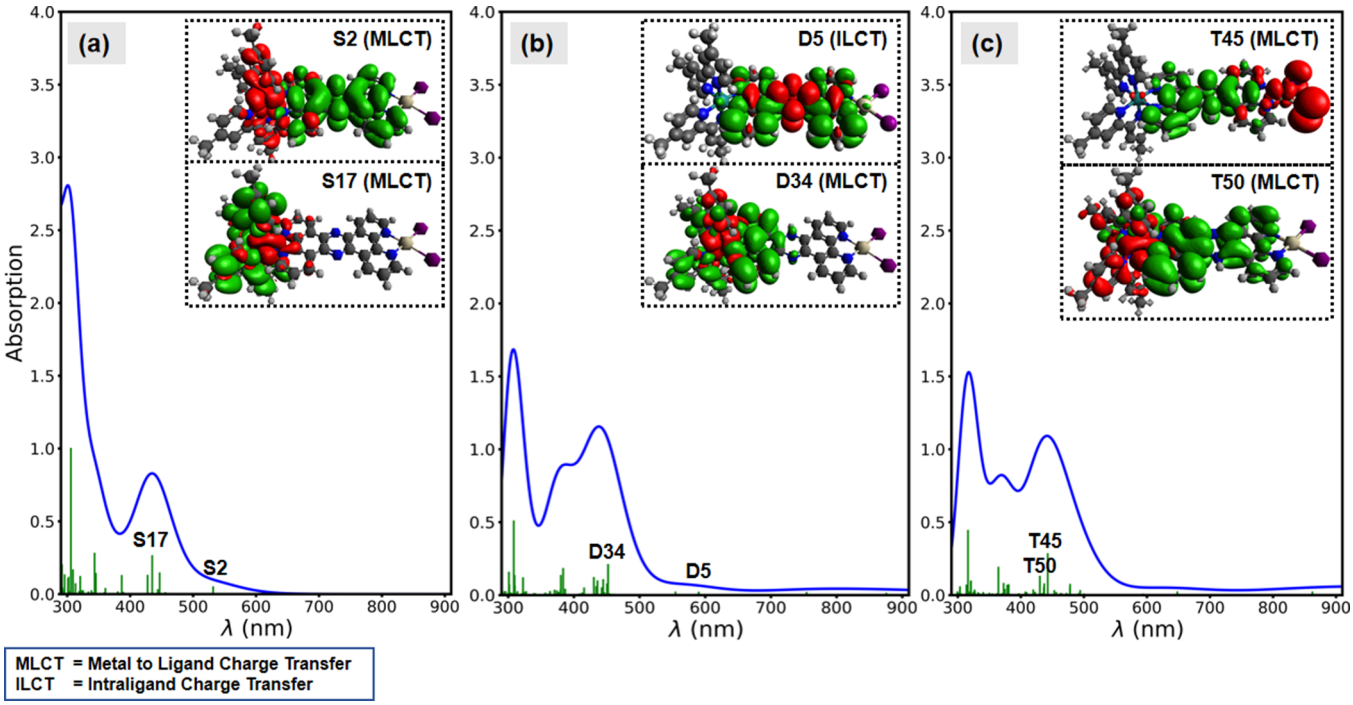

Figure 2. Absorption spectra of the intermediates **1** (panel a), **4** (b), and **6** (c). In addition, the most important excited states, together with their excitation-induced charge density difference, are shown. The excitation direction corresponds to the transition from red to green.

https://doi.org/10.1021/acscatal.6c03235
ACS Catal. XXXX, XXX, XXX–XXX

NEt_3H^+ to form the intermediate **4** is slightly exothermic, only hindered by a moderate energy barrier of 0.49 eV. This process is a bit more favorable than the bridge protonation of intermediate **2** with an activation barrier of 0.56 eV. According to our calculations, upon activation, the structure of NEt_3H^+ becomes modified to avoid the steric interaction with $RuPtI_2$, resulting in a **TS3-4** transition state geometry with a N–H bond length of 1.02 Å and a bond angle of 149.3°, relative to the plane of the bridging ligand (see Scheme 2). This particular mechanism proceeding through intermediate **4** is in good agreement with the experimental findings,[9,27,32] thus supporting the hypothesis that the single protonation of the bridging ligand is an intermediate step in the photocatalytic process. It should be noted that the calculated proton-transfer energetics may be affected by the local solvation environment. Explicit solvation was not considered in this work because it would substantially increase the computational cost and is challenging to implement meaningfully for the mixed solvent system employed here. Accordingly, the present calculations are intended to provide semiquantitative mechanistic insight.

According to our determination of the pK_a values, intermediate **4** remains inactive for any HER step; however, this intermediate has a highly acidic pK_a value of −3.3 for the protonated Pt center. Furthermore, the second protonation of the bridging ligand of intermediate **4** is associated with a pK_a of 7.7, which is still lower than the pK_a of NEt_3H^+. According to experiments,[9,15,27,32,34,84] a significant decline in the catalytic activity is observed, which might be due to the two-fold protonation of the bridging ligand. Obviously, the fully protonated bridging ligands correspond to the deactivated state caused by the lack of unpaired electrons.[33,85] According to our calculations, the deactivation of the photocatalyst should not occur after reaction step Rxn III. In order to understand this, we highlight the role of the sacrificial electron donor (NEt_3) used in this reaction. Besides its function as an electron supplier, the basic pK_a value of 17.6 of NEt_3H^+ also serves as a proton regulator. If an electron donor with a lower pK_a value of, say, 9.0 is chosen, $RuPtI_2$ in its intermediate state **4** would become deactivated by the second protonation of the bridging ligand.

Furthermore, we found from the TD-DFT calculations that the oscillator strength of the ligand-to-metal charge transfer (LMCT) from the bridging ligand to the Pt catalyst in the intermediate configurations **3** and **4** is zero (see Tables S3 and S4). As a result, the LMCT process may not occur at all or will proceed very slowly. This has been demonstrated by performing photoelectrochemistry measurements by Müller and coworkers on the reduced form of $RuPtI_2$.[27] Based on this work, the excitation process of the reduced $RuPtI_2$ ends with charge accumulation on the bipyridine moiety bound to the catalyst,[27] instead of on the Pt catalyst itself. Therefore, it can be concluded that the LMCT process in the intermediates **3** and **4** plays almost no role in a potential protonation event at the Pt atom.

As intermediate **4** is not an active species, the photocatalytic process has to be continued by a second excitation process. According to Figure 2b, the maximum transition probability of intermediate **4** occurs at a wavelength that corresponds to ^{2}MLCT excitation from the ruthenium metal center to the ligands. Thus, the intersystem crossing (ISC) and vibrational cooling (VC) from the doublet into the quartet state become allowed,[86−88] forming intermediate **5**. This transition is associated with a significant increase of the pK_a for the second protonation step to roughly 14, both at the second pyrazine nitrogen atom and at the Pt center. However, the doubly protonated complex still only exists in very small concentrations because the pK_a values are still smaller by three units than the pK_a of NEt_3H^+.

The subsequent electron transfer from the NEt_3 reducing agent is slightly exergonic by −0.33 eV (Scheme 2). This results in the formation of a doubly reduced triplet state, intermediate **6**. According to the Mulliken charge analysis, the excess electron from the donor becomes located at the bridge site with a small spillover onto the catalyst. The pK_a of this doubly reduced intermediate increases slightly to 15.5 with a preference for protonation at the Pt site. This is already reasonably close to the pK_a of 17.6 of the proton donor and, thus, may allow for the presence of a minor concentration of the doubly protonated complex with one proton at the bridging ligand and one at the catalyst. The reaction energy for this proton transfer is slightly endergonic by 0.15 eV and associated with a moderate activation barrier of 0.66 eV (see Scheme S4). Therefore, the protonation of intermediate **6** can proceed at a slow rate. However, this Pt–H hydride is not yet active for hydrogen evolution since the H–H bond formation is still strongly endergonic by 1.48 eV (see Scheme S4). Thus, at least a third reduction is needed to facilitate hydrogen evolution. Similar observations have also been reported for the HER with $[(bpy)Rh(Cp^*)X]^{n+}$-based catalysts under non-acidic conditions.[89−93]

Interestingly, the higher intensity of the ^{2}MLCT transitions of intermediate **4** is crucial for the photocatalytic step. Assuming that the intra-ligand charge transfer (^{2}ILCT) and ligand-to-ligand charge transfer (^{2}LLCT) transitions have higher oscillator strengths than the ^{2}MLCT state, the intersystem crossing (ISC) process will be much slower and the reduction process would favor a doubly reduced singlet state, intermediate **13** (see Scheme S2 for details), instead of the triplet state intermediate **6**. The formation of a singlet spin state (intermediate **13**) renders the second nitrogen atom a stronger base compared to the preferred triplet state, i.e., the pK_a increases from 14.5 in intermediate **6** to 24.2 in intermediate **13**. Accordingly, the bridging ligand would be doubly protonated under reaction conditions according to Scheme 3. Thus, avoiding the low-spin route by switching off ^{2}ILCT and ^{2}LLCT transitions[9,84] in Rxn IV is crucial for avoiding catalyst deactivation. It is noteworthy that under electrochemical conditions, which can only proceed through the more stable low-spin states, this catalyst would therefore be subject to rapid deactivation. More generally, we emphasize that this competition between spin states, and consequently the predicted preference for the productive triplet pathway over the deactivating singlet pathway, depends on the calculated relative energetic ordering of these states, which may be sensitive to the choice of density functional. This mechanistic picture should therefore be interpreted qualitatively, as indicative of a competition between accessible spin states, rather than as a quantitatively definitive prediction.

Based on our calculations, the third reduction is initiated by photoexcitation at 443 nm. After an intersystem crossing and vibrational cooling from the triplet to the quintet state, intermediate **7** is obtained. The excitation corresponds to a charge transfer from the Ru and partly the Pt center to the surrounding ligands (T45 and T50 in Figure 2c). The Mulliken charge analysis indicates an electron transfer of around 0.6e from the photosensitizer toward the bridging ligand. The triplet-to-quintet

https://doi.org/10.1021/acscatal.6c03235
ACS Catal. XXXX, XXX, XXX−XXX

Scheme 3. Possible Reaction Mechanism for the Double Protonation of the Bridging Ligand

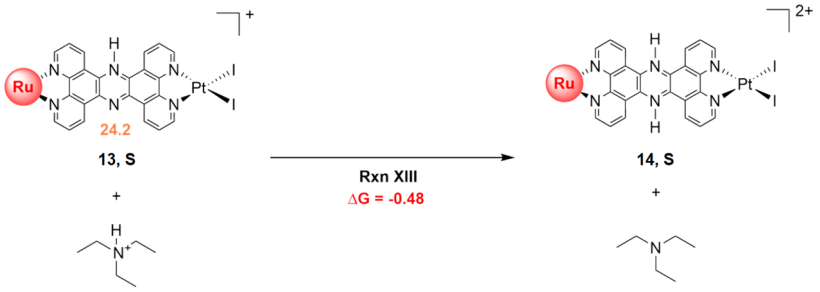

excitation results in a slight increase of the pK_a at the Pt site from 15.5 to 16.6, while at the same, it decreases the pK_a of the second pyrazine nitrogen by a similar amount to 13.0. Thus, double protonation of the bridge is thermodynamically significantly less favorable. In addition, the higher basicity of the Pt catalyst increases the concentration of the protonated Pt–H hydride species, which is important for the subsequent H_2 formation. The reaction energy for proton transfer is 0.07 eV with a moderate activation barrier of 0.54 eV. According to our calculations, the Pt atom is elevated toward the N–H bond of NEt_3H^+ to avoid steric interaction in the transition state (Scheme 2). Moreover, the protonation changes the coordination sphere around the Pt center from square planar to tetragonal bipyramidal with an iodide ligand in the axial position and the hydrogen atom in the planar position. This configuration is more stable than the one with the hydrogen atom in the axial position, with an energy difference of approximately 0.34 eV. Meanwhile, the configuration with both iodine atoms in the planar positions and the hydrogen atom in the axial position was not observed, as the geometry optimization process consistently converged to the configuration with the lowest energy. The protonation is followed by a reduction of the bridging ligand of the complex through oxidation of NEt_3 with a change in Gibbs free energy of –0.03 eV to form intermediate **9**.

We note that this preference for the equatorial over the axial protonation site is because the lifetime of the axial hydride with respect to reverse proton transfer (~24 ps, see detailed calculation in the SI) is too short to allow the subsequent electron-transfer step from the electron donor to transition metal complexes, which is estimated from literature values to occur on the order of hundreds of picoseconds to hundreds of nanoseconds,[94−99] to compete effectively. The equatorial hydride, by contrast, exhibits a substantially longer lifetime (~13 μs) and is therefore considered the catalytically relevant intermediate in this work. However, we would like to remark that this preference is not necessarily general for all platinum complexes because a change in proton source, ligand, or solvent composition could render the axial protonation site more favorable than the equatorial one.

Intermediate **9** corresponds to the final state before the formation of molecular hydrogen occurs. As mentioned above, there are two possible pathways in the hydrogen formation process: the Volmer–Tafel and Volmer–Heyrovsky paths.[65−73] The necessary first step in both mechanisms, the Volmer reaction, has already occurred at Rxn VII. In the Tafel mechanism, a second proton binds to the catalyst, followed by the recombinative desorption of the two hydrogen atoms. According to the rules of organometallic complex formation,[100] only the axial position can act as the available site for the second proton to form an octahedral conformation.

However, the pK_a of the second proton at Pt is 8.4 (see intermediate **9** in Scheme 1), corresponding to a highly unfavorable Gibbs free energy of reaction of 0.66 eV for proton transfer from NEt_3H^+ according to Scheme 4 with pK_a = 17.6. This large thermodynamic penalty strongly suppresses the equilibrium population of the doubly protonated intermediate. Thus, this species is expected to be only negligibly populated at equilibrium. Note that this is in analogy with the findings for the HER on platinum surfaces in heterogeneous catalysis, where no PtH_2 complexes are found on Pt surfaces.[101] It is important to note that this thermodynamic argument is distinct from the kinetic feasibility of the underlying proton-transfer step. Due to the light mass of the proton, a tunneling contribution to the proton transfer appears possible. However, quantum dynamical simulations of the hydrogen reaction probability on

Scheme 4. Hypothetical Scheme for the Double Protonation of the Catalyst

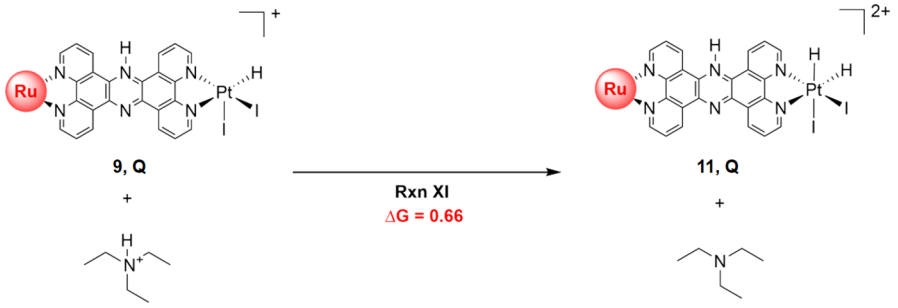

https://doi.org/10.1021/acscatal.6c03235
ACS Catal. XXXX, XXX, XXX–XXX

surfaces have demonstrated that the exponentially suppressed tunneling probability through a relatively high barrier hardly contributes to the overall reaction probability,[102] whereas zero-point effects might in fact play a role.

In particular, it does not, by itself, preclude formation of the intermediate. Potential contributions from hydrogen tunnelling concern the kinetic barrier associated with the formation of this state, rather than its thermodynamic stability or equilibrium population. Therefore, while tunnelling may facilitate the proton-transfer step kinetically, it does not alter the substantial thermodynamic penalty of 0.66 eV associated with the formation of the doubly protonated species. However, the pK_a of the second proton at Pt is 8.4 (see intermediate **9** in Scheme 1) and thus far too low to allow for the proton transfer from NEt_3H^+, which has a pK_a of 17.6 or a Gibbs free energy of reaction of 0.66 eV according to Scheme 4, even considering possible hydrogen tunneling contributions.

A significant decrease in pK_a compared to the first Pt–H bond is in good agreement with general trends for multiprotonic acids[100] and is a result of the decrease in electron density at the bridging ligand and the Pt after the first protonation by 0.46e and 0.15e, respectively (see Rxn VII in Figure 3). Nevertheless, hydrogen evolution from such a doubly protonated species would be feasible as it requires only to overcome a moderate barrier of 0.50 eV. However, a direct Tafel-like mechanism can be excluded for $RuPtI_2$, as already indicated above, owing to the very low concentration of the doubly protonated species at the Pt center, even though it is kinetically feasible.

This leaves only a Heyrovsky mechanism as the possible path to H_2 formation. Indeed, the direct attack of a proton at the Pt–H site is, with 0.08 eV, almost thermoneutral (see Rxn IX in Scheme 2). Additionally, the activation barrier of Rxn IX is 0.68 eV. The moderate barrier is associated with the planar position of the Pt–H hydride and the attack of NEt_3H^+ from the axial direction. This configuration allows for the stabilization of the H–H species through an interaction between the d-orbitals of the Pt atom and the σ bond of the H–H species. However, the steric interactions between the ethyl groups of NEt_3H^+ and the phenanthroline group surrounding the $RuPtI_2$ center slow down the proton transfer. According to a Mulliken charge analysis, the proton transfer process and the formation of the H_2 molecules in Rxn IX require an electron transfer of 0.8e and 0.2e from the bridging ligand and the Pt catalyst of intermediate **9**, respectively. Overall, this Mulliken charge and spin-density analysis is consistent with the bridging ligand acting not only to connect the photosensitizer and catalyst but also as a site of electron storage prior to its use in H_2 formation.[103] However, we note that this interpretation is based on qualitative charge and spin-density distributions rather than a rigorous quantitative decomposition of electron localization.

Although molecular hydrogen is produced from intermediate **9**, deactivation can also occur at this intermediate. We find the second protonation step at the bridge to be associated with a pK_a of 15.0. This is reasonably close to the pK_a of the proton donor, NEt_3H^+, to allow for some double protonation of the bridge. Consequently, proton transfer is feasible here, with a reaction slightly endergonic by 0.18 eV but hindered by a rather high activation barrier of 0.82 eV. After formation of the protonated bridge species, hydrogen evolution is hindered by a very high activation barrier of 1.13 eV and is therefore effectively inhibited (see Scheme S10 for details). Although the reaction is slow, the deactivation process in $RuPtI_2$ cannot be avoided and may at least partly explain the experimentally observed catalyst deactivation after 48 h of operation.[9,15,32,34,84]

Returning to the photocatalytic cycle shown in Scheme 1, we note that once the H–H bond is formed, H_2 is immediately released from the catalyst under formation of a trigonal pyramidal coordination sphere around Pt, yielding intermediate **10**. According to the spin analysis (see Figure S2), the total spin densities on the bridging ligand and PtI_2 of intermediate **10** are 1.27 and 1.73, respectively. In other words, there is roughly one unpaired electron on the bridging ligand and two unpaired electrons on the PtI_2 catalyst due to the non-square planar configuration. Furthermore, the I–Pt–I configuration in $RuPtI_2$ is similar to the CO–Pt–Cl configuration in the triplet metal-centered (^{3}MC) state of Pt(ppy)(CO)(Cl), as calculated by Escudero and coworkers.[104,105] Thus,

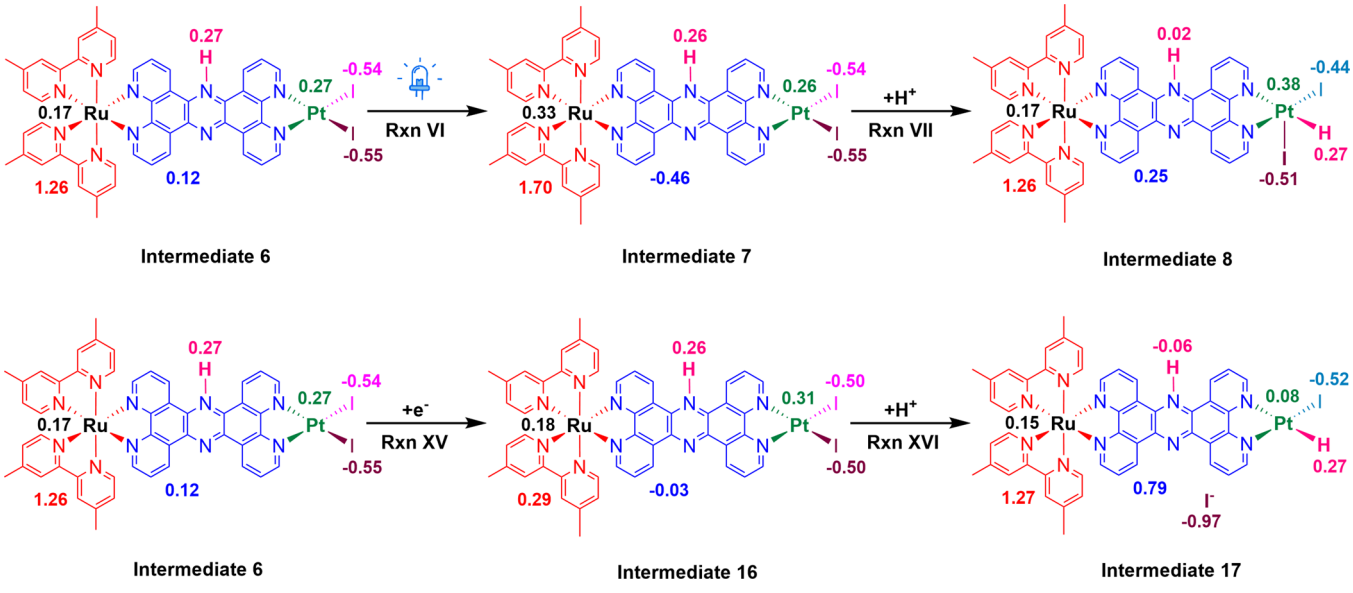

Figure 3. Mulliken charge of intermediates in two reactions: catalyst activation (top) and loss of the iodide ligand reaction (bottom).

https://doi.org/10.1021/acscatal.6c03235
ACS Catal. XXXX, XXX, XXX–XXX

intermediate **10** can be considered as a quartet metal-centered (^{4}MC) state of $RuPtI_2$.[104,105] Afterward, the photocatalytic cycle ends with the restoration of its square planar coordination geometry (see Rxn X in Scheme 2). This restoration is followed by spin crossover from quartet to doublet,[104−107] forming intermediate **4**.

It is, of course, an interesting issue to identify the rate-limiting step in this catalytic cycle. As can be seen in Scheme 1, there are some reaction steps associated with barriers between about 0.5 and 0.7 eV. However, to obtain a qualitative estimate of the reaction kinetics, we employed the Eyring equation[108−110] to calculate the rate constants for the elementary steps associated with the transition states. The calculated rate constants are 2.26×10^5 s^{-1} for **TS3-4**, 4.7×10^3 s^{-1} for **TS7-8**, and 1.9×10^1 s^{-1} for **TS9-10**. These results indicate that the **TS9-10** step is substantially slower than the preceding elementary steps and is therefore expected to be the rate-limiting step within the proposed catalytic cycle. Alternatively, one could address kinetic isotope effects by performing quantum nuclear dynamics simulations,[111] which, however, is also numerically extremely demanding. In addition, from a photophysical perspective, reliable information regarding the lifetimes and populations of the higher-spin intermediates involved in the singly, doubly, and triply reduced states (intermediates **2**, **5**, **8**, and **10**) would also be required for the kinetic study. These parameters are essential for accurately determining the steady-state concentrations of reactive intermediates and the overall catalytic rate. A rigorous treatment of the spin-state dynamics and electronic structures of these intermediates would further require computationally demanding multireference approaches, which are currently beyond the feasible computational scope for this system size. Furthermore, we like to emphasize that the present computational work focuses on the adiabatic ground-state proton- and electron-transfer chemistry captured in Scheme 1.

Besides the mechanism of the light-driven hydrogen evolution reaction (HER) of $RuPtI_2$, the prevention of degradation is of high relevance and can be unraveled in our mechanistic first-principles study. According to our calculations, the ability to access higher spin states through intersystem crossing avoids catalyst degradation, as shown for the conversion of intermediate **4** into **6**. Assume a situation in which, starting from intermediate **6**, the ^{3}ILCT and ^{3}LLCT transitions would have the highest harmonic oscillator strengths. Similar to the previous case, this would again slow down the intersystem crossing and thus inhibit the transition into a quintet state. Accordingly, the more stable triply reduced doublet state, intermediate **16**, is formed. The Pt site of this species is strongly basic with a pK_a of 33.1. While this is, to some degree, even beneficial, we also find that protonation of the Pt site in a doublet state immediately results in the release of an I^- ligand (intermediate **17** in Scheme 5).

The degradation process in Rxn XVI can be explained by the changes in Mulliken charges in Figure 3. The release of the iodide ligand is initiated by the formation of intermediate **16** through an electron transfer. Here, excess electron density from the donor accumulates on the photosensitizer, specifically on the bipyridine ligand. One additional electron becomes stored at the $Rubpy_2$ unit in the doublet state compared to the quartet state. Upon Pt–H bond formation, 1.8e electrons are transferred from the bipyridine and bridging ligand to the active site. Of these electrons, 0.7e are specifically utilized for proton reduction, while the remaining electrons are allocated for the release of the iodide ligand as I^-. This result supports the findings from previous studies that the decomposition process in PtX_2 catalysts (where X = Cl and I) occurs when the catalyst acquires two electrons.[103,112,113] On the other hand, catalyst degradation is not observed when only one electron is transferred to the catalyst. Note that the low-spin decomposition path can again not be avoided under electrochemical conditions since it does not allow the excitation to the stable quartet state. Similarly, this path is also the preferred route if the bridging ligand would remain unprotonated. Hence, single protonation of the bridging ligand is critical for maintaining catalyst stability by deactivating the ILCT and LLCT transitions and allowing the ISC process to access the higher spin state, which prevents degradation.

Another alternative to avoid degradation is utilizing the optical properties of intermediate **16** (see Scheme S8 for details). According to our TD-DFT calculations, the wavelength of maximum absorption of this intermediate at a value of 449 nm is characterized by ^{2}MLCT (see Table S8 in the SI). Therefore, intersystem crossing from doublet to quartet is allowed to form intermediate **8**. Based on previous work,[9,34,86,114−117] the intersystem crossing in ruthenium complexes occurs rapidly with a timescale below 1 ps. Meanwhile, protonation at the Pt center occurs at a timescale above 1 ps,[118−120] depending on the reaction environment and proton concentration. Thus, the ISC process is much faster than protonation, and catalyst degradation on the triply reduced doublet state can be evaded through this excitation and the transition into the more stable quartet state. Indeed, catalyst degradation may represent one possible pathway affecting the performance of Ru–Pt-based catalysts with different bridging ligands, particularly for ligands that cannot be protonated.[19,20,121−125] However, the specific degradation pathways may depend on the nature of the bridging ligand. A very intriguing correlation between the sequence of redox events and stability of the platinum-complex-based catalyst has recently been put forward, i.e., if the first reduction is

Scheme 5. Release of an I^- Ligand from the Catalyst upon Protonation of the Pt Site of Intermediate 16

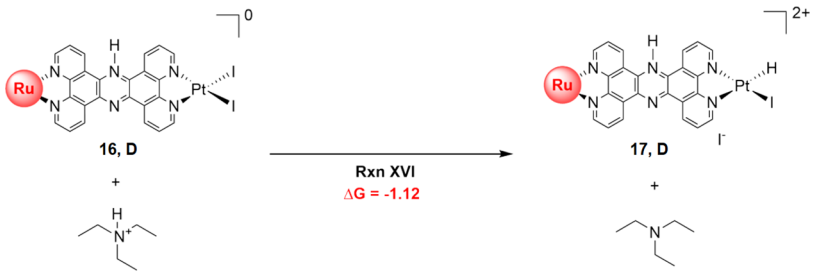

https://doi.org/10.1021/acscatal.6c03235
ACS Catal. XXXX, XXX, XXX−XXX

ligand-based, then enhanced stability of the molecularly defined catalyst may be anticipated.[19] The results presented here explicitly focus on ligand architectures, tpphz, which possess the capability of being the easiest to reduce if coordinated to a platinum(II) center; however, here, they are accompanied by the capability of protonation. More detailed investigations into the generality of the redox sequence line of argumentation are required.

CONCLUSIONS

In conclusion, based on state-of-the-art first-principles calculations, we have presented a complete catalytic cycle of the photocatalytic hydrogen evolution reaction on a photochemical molecular device. To the best of our knowledge, such a complete catalytic cycle has not been reported before. The proposed reaction mechanism has been based on the existing experimental information in a consistent way, filling the gaps by results of state-of-the-art quantum chemical calculations. Our study clearly reveals the important role of the bridging ligand between the photosensitizer and the catalyst in the hydrogen evolution reaction. It furthermore provides a rational explanation for the recently discovered induction period for activating the photochemical molecular device. It highlights the correlation between light-driven electron transfer from the photocenter to the bridging ligand and subsequent protonation of the bridging ligand, which has been observed experimentally to play a pivotal role in determining photocatalytic activity. Only this step enables the formation of hydrogen at the later stages of the catalytic cycle. A fundamentally new perspective on the light-driven catalytic process is our key finding that the whole catalytic cycle does not progress as previously assumed via a starting singlet configuration, which then progresses via a doublet intermediate to a final singlet, twofold reduced state located at the Pt–H bond. Our findings show a very different sequence of intermediates forming a doublet state within the induction phase of catalysis, which then progresses to even higher multiplicity intermediates. Furthermore, these higher-spin states are also crucial for preventing degradation of the photoactive complex.

The reaction proceeds through an induction phase step in which a light-driven electron transfer to the bridging ligand is followed by protonation of the basic nitrogen moiety. Subsequent two-fold light-driven electron transfer across this already one-fold reduced bridge is followed by a Volmer–Heyrovsky type hydrogen evolution mechanism, in which the sacrificial donor acts as a proton regulator. The dual function of the sacrificial electron donor, acting as a reducing agent and, at the same time, as a regulator of proton concentration, and therefore providing a dual tuning of the photocatalytic activity, becomes very apparent in this work. The hydrogen molecule is eventually formed from a proton in solution and a hydrogen atom bound to the Pt-based catalyst, together with an electron transfer from both the bridging ligand and the catalyst of the photochemical molecular device. This is consistent with the notion that the bridging ligand also acts as an electron storage, thus being directly involved in the hydrogen evolution reaction. Besides, it turns out that the single protonation of the bridging ligand is critical for maintaining catalyst stability. The atomic-level understanding of the crucial processes and steps in the photocatalytic hydrogen evolution reaction obtained in this quantum chemical study should be instrumental in further improving the activity of photomolecular devices.

The presented findings clearly suggest that a reversible proton-accepting sphere as part of the bridging ligand architecture is very relevant as this supports the crucial one electron reduced state of the photocatalyst, which is the catalytically active state. An acridine-like architecture, instead of the phenazine-like unit in tpphz, could provide this property while, at the same time, raising the LUMO of the central sphere, thus reducing thermal activation energies for the intramolecular electron transfer. More fundamentally, it is very apparent from the presented results that intramolecular photocatalysis is proceeding via doublet or even higher spin states. This prediction would imply that electron paramagnetic resonance methods like transient electron paramagnetic resonance could provide essential spectroscopic details for the mechanism, as nearly all intermediates of the catalytic cycle possess unpaired electrons. It furthermore opens a new perspective on the requirements for soft matter/surface immobilization, as stabilization of radical intermediates would be required, as they represent the catalytically active state of the photocatalyst.

ASSOCIATED CONTENT

Supporting Information

The Supporting Information is available free of charge at https://pubs.acs.org/doi/10.1021/acscatal.6c03235.

Description of the methodology for calculating pKa values, details of the kinetic calculations, Mulliken charge and spin density analysis of all reaction intermediates, comparison of measured and calculated absorption spectra for a range of DFT functionals, internal bond lengths and bond angles of all considered intermediates; reaction energetics of further considered reaction schemes, kinetic analysis of the axial versus the equatorial protonation of the catalyst, properties of selected electronic transitions, and link to the repository providing the structural parameters of all intermediates (DOCX)

AUTHOR INFORMATION

Corresponding Author

Axel Groß – *Institute of Theoretical Chemistry, Ulm University, Ulm 89081, Germany; Helmholtz Institute Ulm (HIU), Electrochemical Energy Storage, Ulm 89069, Germany;* orcid.org/0000-0003-4037-7331; Email: axel.gross@uni-ulm.de

Authors

Miftahussurur Hamidi Putra – *Institute of Theoretical Chemistry, Ulm University, Ulm 89081, Germany*

Alexander K. Mengele – *Institute of Inorganic Chemistry I, Materials and Catalysis, Ulm University, Ulm 89081, Germany;* orcid.org/0000-0001-6496-3429

Benedikt Bagemihl – *Institute of Inorganic Chemistry I, Materials and Catalysis, Ulm University, Ulm 89081, Germany*

Sven Rau – *Institute of Inorganic Chemistry I, Materials and Catalysis, Ulm University, Ulm 89081, Germany;* orcid.org/0000-0001-9635-6009

Michael Busch – *Institute of Theoretical Chemistry, Ulm University, Ulm 89081, Germany; Division of Materials Science, Department of Engineering Sciences and Mathematics,Luleå University of Technology, Luleå 971 87, Sweden; Wallenberg*

Initiative Materials Science for Sustainability (WISE), Luleå University of Technology, Luleå 971 87, Sweden; orcid.org/0000-0003-3883-2868

Complete contact information is available at: https://pubs.acs.org/doi/10.1021/acscatal.6c03235

Notes

The authors declare no competing financial interest.

■ ACKNOWLEDGEMENTS

Computer time on the JUSTUS cluster at Ulm University provided by the bwHPC initiative and the bwHPC-C5 project funded by the Baden-Württemberg government (MWK) and the German Research Foundation (DFG) under Grant No. INST 40/575-1 FUGG (JUSTUS 2 cluster) is gratefully acknowledged. M.H.P., A.K.M., B.B., S.R., and A.G. thank the DFG for financial support through Project A1 and C5 of the Transregional Collaborative Research Centre TRR234 CataLight (Project No.364549901). M.B. acknowledges financial support through the Dr. Barbara-Mez-Starck foundation and the Wallenberg Initiative Materials Science for Sustainability (WISE) funded by the Knut and Alice Wallenberg Foundation (KAW). This work contributes to the research performed at CELEST (Center for Electrochemical Energy Storage Ulm-Karlsruhe).

■ REFERENCES

(1) Schlögl, R. The Role of Chemistry in the Energy Challenge. *ChemSusChem* **2010**, *3*, 209–222.
(2) Grätzel, M. Photoelectrochemical cells. *Nature* **2001**, *414*, 338–344.
(3) Dalle, K. E.; Warnan, J.; Leung, J. J.; Reuillard, B.; Karmel, I. S.; Reisner, E. Electro- and Solar-Driven Fuel Synthesis with First Row Transition Metal Complexes. *Chem. Rev.* **2019**, *119*, 2752–2875.
(4) Staffell, I.; Scamman, D.; Abad, A. V.; Balcombe, P.; Dodds, P. E.; Ekins, P.; Shah, N.; Ward, K. R. The role of hydrogen and fuel cells in the global energy system. *Energy Environ. Sci.* **2019**, *12*, 463–491.
(5) Mori, S.; Hashimoto, R.; Hisatomi, T.; Domen, K.; Saito, S. Artificial photosynthesis directed toward organic synthesis. *Nat. Comm.* **2025**, *16*, 1797.
(6) Gisriel, C. J.; Flesher, D. A.; Shen, G.; Wang, J.; Ho, M.-Y.; Brudvig, G. W.; Bryant, D. A. Structure of a photosystem I-ferredoxin complex from a marine cyanobacterium provides insights into far-red light photoacclimation. *J. Biol. Chem.* **2022**, *298*, 101408.
(7) Zedler, L.; Wintergerst, P.; Mengele, A. K.; Müller, C.; Li, C.; Dietzek-Ivanšić, B.; Rau, S. Outpacing conventional nicotinamide hydrogenation catalysis by a strongly communicating heterodinuclear photocatalyst. *Nat. Comm.* **2022**, *13*, 2538.
(8) Ozawa, H.; Sakai, K. Photo-hydrogen-evolving molecular devices driving visible-light-induced water reduction into molecular hydrogen: structure–activity relationship and reaction mechanism. *Chem. Commun.* **2011**, *47*, 2227.
(9) Pfeffer, M. G. et al. Active repair of a dinuclear photocatalyst for visible-light-driven hydrogen production. *Nat. Chem.* **2022**, *14*, 500–506.
(10) Manbeck, G. F.; Fujita, E.; Brewer, K. J. Tetra- and Heptametallic Ru(II), Rh(III) Supramolecular Hydrogen Production Photocatalysts. *J. Am. Chem. Soc.* **2017**, *139*, 7843–7854.
(11) Chen, S.; Li, K.; Zhao, F.; Zhang, L.; Pan, M.; Fan, Y.-Z.; Guo, J.; Shi, J.; Su, C.-Y. A metal-organic cage incorporating multiple light harvesting and catalytic centres for photochemical hydrogen production. *Nat. Comm.* **2016**, *7*, 13169.
(12) Li, G.; Zhu, D.; Wang, X.; Su, Z.; Bryce, M. R. Dinuclear metal complexes: multifunctional properties and applications. *Chem. Soc. Rev.* **2020**, *49*, 765–838.
(13) Andreiadis, E. S.; Chavarot-Kerlidou, M.; Fontecave, M.; Artero, V. Artificial Photosynthesis: From Molecular Catalysts for Light-driven Water Splitting to Photoelectrochemical Cells. *Photochem. Photobiol.* **2011**, *87*, 946–964.
(14) Costabel, D.; De, R.; Jacobi, F.; Eichhorn, J.; Hotzel, K.; Nabiyan, A.; Neumann, C.; Turchanin, A.; Kupfer, S.; Schacher, F. H.; Rau, S.; Dietzek-Ivanšić, B.; Peneva, K. Bridging Platinum and Palladium to Bipyridine-Annulated Perylene for Light-Driven Hydrogen Evolution. *ACS Catal.* **2023**, *13*, 7159–7169.
(15) Pfeffer, M. G.; Schäfer, B.; Smolentsev, G.; Uhlig, J.; Nazarenko, E.; Guthmuller, J.; Kuhnt, C.; Wächtler, M.; Dietzek, B.; Sundström, V.; Rau, S. Palladium versus Platinum: The Metal in the Catalytic Center of a Molecular Photocatalyst Determines the Mechanism of the Hydrogen Production with Visible Light. *Angew. Chem., Int. Ed.* **2015**, *54*, 5044–5048.
(16) Putra, M. H.; Bagemihl, B.; Rau, S.; Groß, A. Prediction of Strong Solvatochromism in a Molecular Photocatalyst. *Chem. Eur. J.* **2024**, *30*, e202302643.
(17) Tschierlei, S.; Presselt, M.; Kuhnt, C.; Yartsev, A.; Pascher, T.; Sundström, V.; Karnahl, M.; Schwalbe, M.; Schäfer, B.; Rau, S.; Schmitt, M.; Dietzek, B.; Popp, J. Photophysics of an Intramolecular Hydrogen-Evolving Ru-Pd Photocatalyst. *Chem. Eur. J.* **2009**, *15*, 7678–7688.
(18) Sen, A.; Putra, M. H.; Biswas, A. K.; Behera, A. K.; Groß, A. Insight on the choice of sensitizers/dyes for dye sensitized solar cells: A review. *Dyes Pigments* **2023**, *213*, 111087.
(19) Lämmle, M.; Mengele, A. K.; Shillito, G. E.; Kupfer, S.; Rau, S. Stability of Catalytic Centres in Light-Driven Hydrogen Evolution by Di- and Oligonuclear Photocatalysts. *Chem. Eur. J.* **2023**, *29*, e202202722.
(20) Lämmle, M.; Pilz, T. D.; Kutta, R. J.; Müßler, M.; Mengele, A. K.; Görls, H.; Heinemann, F. W.; Rau, S. Insights into the different mechanistic stages of light-induced hydrogen evolution of a 5, 5'-bisphenanthroline linked RuPt complex. *Dalton Trans.* **2022**, *51*, 15282–15291.
(21) Zedler, L.; Guthmuller, J.; Rabelo de Moraes, I.; Kupfer, S.; Krieck, S.; Schmitt, M.; Popp, J.; Rau, S.; Dietzek, B. Resonance-Raman spectro-electrochemistry of intermediates in molecular artificial photosynthesis of bimetallic complexes. *Chem. Commun.* **2014**, *50*, 5227.
(22) Giannoudis, E.; Bold, S.; Müller, C.; Schwab, A.; Bruhnke, J.; Queyriaux, N.; Gablin, C.; Leonard, D.; Saint-Pierre, C.; Gasparutto, D.; Aldakov, D.; Kupfer, S.; Artero, V.; Dietzek, B.; Chavarot-Kerlidou, M. Hydrogen Production at a NiO Photocathode Based on a Ruthenium Dye–Cobalt Diimine Dioxime Catalyst Assembly: Insights from Advanced Spectroscopy and Post-operando Characterization. *ACS Appl. Mater. Interfaces* **2021**, *13*, 49802–49815.
(23) Durovic, M.; Hnat, J.; Bouzek, K. Electrocatalysts for the hydrogen evolution reaction in alkaline and neutral media. A comparative review. *J. Power Sources* **2021**, *493*, 229708.
(24) Luo, L.; Zhou, X.; Chen, Y.; Sun, F.; Wang, L.; Tang, Q. Ligand-induced changes in the electrocatalytic activity of atomically precise Au_{25} nanoclusters. *Chem. Sci.* **2025**, *16*, 3598–3610.
(25) Martynow, M.; Kupfer, S.; Rau, S.; Guthmuller, J. Excited state properties of a series of molecular photocatalysts investigated by time dependent density functional theory. *Phys. Chem. Chem. Phys.* **2019**, *21*, 9052–9060.
(26) Staniszewska, M.; Kupfer, S.; Guthmuller, J. Effect of the Catalytic Center on the Electron Transfer Dynamics in Hydrogen-Evolving Ruthenium-Based Photocatalysts Investigated by Theoretical Calculations. *J. Phys. Chem. C* **2019**, *123*, 16003–16013.
(27) Müller, C.; Friedländer, I.; Bagemihl, B.; Rau, S.; Dietzek-Ivanšić, B. The electron that breaks the catalyst's back - excited state dynamics in intermediates of molecular photocatalysts. *Phys. Chem. Chem. Phys.* **2021**, *23*, 27397–27403.

(28) Baranowska, D.; Kedzierski, T.; Leniec, G.; Zielinska, B.; Mijowska, E. Phase Transition Assisted Photo-, Electro- and Photoelectrocatalytic Hydrogen Evolution in B/MoS_2-Mechanistic Insight. *Chem. Mater.* **2025**, *37*, 3622–3634.
(29) Groß, A. Challenges in the modeling of elementary steps in electrocatalysis. *Curr. Opin. Electrochem.* **2023**, *37*, 101170.
(30) Ogawa, M.; Ajayakumar, G.; Masaoka, S.; Kraatz, H.; Sakai, K. Platinum(II)-Based Hydrogen-Evolving Catalysts Linked to Multipendant Viologen Acceptors: Experimental and DFT Indications for Bimolecular Pathways. *Chem. Eur. J.* **2010**, *17*, 1148–1162.
(31) Yang, X.; Hall, M. B. Mechanism of Water Splitting and Oxygen-Oxygen Bond Formation by a Mononuclear Ruthenium Complex. *J. Am. Chem. Soc.* **2010**, *132*, 120–130.
(32) Klingler, S.; Bagemihl, B.; Mengele, A. K.; Kaufhold, S.; Myllyperkiö, P.; Ahokas, J.; Pettersson, M.; Rau, S.; Mizaikoff, B. Rationalizing In Situ Active Repair in Hydrogen Evolution Photocatalysis via Non-Invasive Raman Spectroscopy. *Angew. Chem., Int. Ed.* **2023**, *62*, e202306287.
(33) Li, M.; Sakong, S.; Gross, A. In Search of the Active Sites for the Selective Catalytic Reduction on Tungsten-Doped Vanadia Monolayer Catalysts supported by TiO_2. *ACS Catal.* **2021**, *11*, 7411–7421.
(34) Pfeffer, M. G.; Kowacs, T.; Wächtler, M.; Guthmuller, J.; Dietzek, B.; Vos, J. G.; Rau, S. Optimization of Hydrogen-Evolving Photochemical Molecular Devices. *Angew. Chem., Int. Ed.* **2015**, *54*, 6627–6631.
(35) Frisch, M. J. et al. *Gaussian16 Revision C.01*; Gaussian Inc.: Wallingford CT, **2016**.
(36) Becke, A. D. Density functional thermochemistry. III. The role of exact exchange. *J. Chem. Phys.* **1993**, *98*, 5648–5652.
(37) Lee, C.; Yang, W.; Parr, R. G. Development of the Colle-Salvetti correlation-energy formula into a functional of the electron density. *Phys. Rev. B* **1988**, *37*, 785–789.
(38) Grimme, S.; Ehrlich, S.; Goerigk, L. Effect of the damping function in dispersion corrected density functional theory. *J. Comp. Chem.* **2011**, *32*, 1456–1465.
(39) Weigend, F.; Ahlrichs, R. Balanced basis sets of split valence, triple zeta valence and quadruple zeta valence quality for H to Rn: Design and assessment of accuracy. *Phys. Chem. Chem. Phys.* **2005**, *7*, 3297–3305.
(40) Weigend, F. Accurate Coulomb-fitting basis sets for H to Rn. *Phys. Chem. Chem. Phys.* **2006**, *8*, 1057–1065.
(41) Boys, S.; Bernardi, F. The calculation of small molecular interactions by the differences of separate total energies. Some procedures with reduced errors. *Mol. Phys.* **1970**, *19*, 553–566.
(42) Veccham, S. P.; Head-Gordon, M. Density Functionals for Hydrogen Storage: Defining the H2Bind275 Test Set with Ab Initio Benchmarks and Assessment of 55 Functionals. *J. Chem. Theory Comput.* **2020**, *16*, 4963–4982.
(43) Brakestad, A.; Wind, P.; Jensen, S. R.; Frediani, L.; Hopmann, K. H. Multiwavelets applied to metal–ligand interactions: Energies free from basis set errors. *J. Chem. Phys.* **2021**, *154*, 214302.
(44) Bligaard, T.; Nørskov, J.; Dahl, S.; Matthiesen, J.; Christensen, C.; Sehested, J. The Brønsted–Evans–Polanyi relation and the volcano curve in heterogeneous catalysis. *J. Catal.* **2004**, *224*, 206–217.
(45) Groß, A. Challenges for ab initio molecular dynamics simulations of electrochemical interfaces. *Curr. Opin. Electrochem.* **2023**, *40*, 101345.
(46) Marenich, A. V.; Cramer, C. J.; Truhlar, D. G. Universal Solvation Model Based on Solute Electron Density and on a Continuum Model of the Solvent Defined by the Bulk Dielectric Constant and Atomic Surface Tensions. *J. Phys. Chem. B* **2009**, *113*, 6378–6396.
(47) Maldonado, A. M.; Basdogan, Y.; Berryman, J. T.; Rempe, S. B.; Keith, J. A. First-principles modeling of chemistry in mixed solvents: Where to go from here? *J. Chem. Phys.* **2020**, *152*, 130902.
(48) Adamo, C.; Jacquemin, D. The calculations of excited-state properties with Time-Dependent Density Functional Theory. *Chem. Soc. Rev.* **2013**, *42*, 845–856.
(49) Laurent, A. D.; Adamo, C.; Jacquemin, D. Dye chemistry with time-dependent density functional theory. *Phys. Chem. Chem. Phys.* **2014**, *16*, 14334–14356.
(50) Reiher, M.; Salomon, O. a. Reparameterization of hybrid functionals based on energy differences of states of different multiplicity. *Theor. Chem. Acc.* **2001**, *107*, 48–55.
(51) Busch, M.; Ahlberg, E.; Ahlberg, E.; Laasonen, K. How to Predict the pK_a of Any Compound in Any Solvent. *ACS Omega* **2022**, *7*, 17369–17383.
(52) Busch, M.; Ahlberg, E.; Laasonen, K. From absolute potentials to a generalized computational standard hydrogen electrode for aqueous and non-aqueous solvents. *Phys. Chem. Chem. Phys.* **2021**, *23*, 11727–11737.
(53) Busch, M.; Ahlberg, E.; Laasonen, K. Universal Trends between Acid Dissociation Constants in Protic and Aprotic Solvents. *Chem. Eur. J.* **2022**, *28*, e202201667.
(54) Ho, J.; Coote, M. L. pKa Calculation of Some Biologically Important Carbon Acids - An Assessment of Contemporary Theoretical Procedures. *J. Chem. Theory Comput.* **2009**, *5*, 295–306.
(55) Ho, J. Predicting pKa in Implicit Solvents: Current Status and Future Directions. *Aust. J. Chem.* **2014**, *67*, 1441.
(56) Casasnovas, R.; Ortega-Castro, J.; Frau, J.; Donoso, J.; Muñoz, F. Theoretical pKa calculations with continuum model solvents, alternative protocols to thermodynamic cycles. *Int. J. Quantum Chem.* **2014**, *114*, 1350–1363.
(57) Ho, J.; Coote, M. L. A universal approach for continuum solvent pK a calculations: are we there yet? *Theor. Chem. Acc.* **2009**, *125*, 3–21.
(58) Muckerman, J. T.; Skone, J. H.; Ning, M.; Wasada-Tsutsui, Y. Toward the accurate calculation of pKa values in water and acetonitrile. *Biochim. Biophys. Acta* **2013**, *1827*, 882–891.
(59) Rossini, E.; Knapp, E.-W. Proton solvation in protic and aprotic solvents. *J. Comput. Chem.* **2016**, *37*, 1082–1091.
(60) Busch, M.; Laasonen, K.; Ahlberg, E. Method for the accurate prediction of electron transfer potentials using an effective absolute potential. *Phys. Chem. Chem. Phys.* **2020**, *22*, 25833–25840.
(61) Mulliken, R. S. Electronic Population Analysis on LCAO–MO Molecular Wave Functions. I. *J. Chem. Phys.* **1955**, *23*, 1833–1840.
(62) Åstrand, P.-O.; Ruud, K.; Mikkelsen, K. V.; Helgaker, T. Atomic Charges of the Water Molecule and the Water Dimer. *J. Phys. Chem. A* **1998**, *102*, 7686–7691.
(63) North, S. C.; Jorgensen, K. R.; Pricetolstoy, J.; Wilson, A. K. Population analysis and the effects of Gaussian basis set quality and quantum mechanical approach: main group through heavy element species. *Front. Chem.* **2023**, *11*, 1152500.
(64) Sotoudeh, M.; Baumgart, S.; Dillenz, M.; Döhn, J.; Forster-Tonigold, K.; Helmbrecht, K.; Stottmeister, D.; Groß, A. Ion Mobility in Crystalline Battery Materials. *Adv. Energy Mater.* **2024**, *14*, 2302550.
(65) Erdey-Grúz, T.; Volmer, M. Zur Theorie der Wasserstoff Überspannung. *Z. Phys. Chem.* **1930**, *150A*, 203–213.
(66) Tafel, J. Über die Polarisation bei kathodischer Wasserstoffentwicklung. *Z. Phys. Chem.* **1905**, *50U*, 641–712.
(67) Heyrovský, J. A theory of overpotential. *Recl. Trav. Chim. Pays-Bas* **1927**, *46*, 582–585.
(68) Schnur, S.; Groß, A. Challenges in the first-principles description of reactions in electrocatalysis. *Catal. Today* **2011**, *165*, 129–137.
(69) Huang, J.; Zhu, X.; Eikerling, M. The rate-determining term of electrocatalytic reactions with first-order kinetics. *Electrochim. Acta* **2021**, *393*, 139019.
(70) Kronberg, R.; Lappalainen, H.; Laasonen, K. Revisiting the Volmer–Heyrovský mechanism of hydrogen evolution on a nitrogen doped carbon nanotube: constrained molecular dynamics versus the nudged elastic band method. *Phys. Chem. Chem. Phys.* **2020**, *22*, 10536–10549.
(71) Chen, Z.; Duan, X.; Wei, W.; Wang, S.; Ni, B.-J. Recent advances in transition metal-based electrocatalysts for alkaline hydrogen evolution. *J. Mater. Chem. A* **2019**, *7*, 14971–15005.

https://doi.org/10.1021/acscatal.6c03235
ACS Catal. XXXX, XXX, XXX–XXX

(72) Faid, A. Y.; Sunde, S. Anion Exchange Membrane Water Electrolysis from Catalyst Design to the Membrane Electrode Assembly. *Energy Technol.* **2022**, *10*, 2200506.
(73) Wu, Z.-P.; Lu, X. F.; Zang, S.-Q.; Lou, X. W. D. Non-Noble-Metal-Based Electrocatalysts toward the Oxygen Evolution Reaction. *Adv. Funct. Mater.* **2020**, *30*, 1910274.
(74) Dinnocenzo, J. P.; Banach, T. E. Deprotonation of tertiary amine cation radicals. A direct experimental approach. *J. Am. Chem. Soc.* **1989**, *111*, 8646–8653.
(75) Carr, C. R.; Vrionides, M. A.; Sosulin, I. S.; Lisouskaya, A.; Ertem, M. Z.; Grills, D. C. Electron Transfer Theory Elucidates the Hidden Role Played by Triethylamine and Triethanolamine during Photocatalysis. *J. Am. Chem. Soc.* **2025**, *147*, 32005–32014.
(76) Habermehl, J.; Nauroozi, D.; Martynow, M.; Vilk, Y. E.; Beranek, R.; Guthmuller, J.; Rau, S. Synthesis and hydrogen evolving catalysis of a panchromatic photochemical molecular device. *Sustain. Energy Fuels* **2020**, *4*, 619–624.
(77) Hartkorn, M.; Kampes, R.; Müller, F.; Zedler, L.; Edwards, A.; Rohland, P.; Mengele, A. K.; Zechel, S.; Hager, M. D.; Dietzek-Ivanšić, B.; Schmitt, M.; Popp, J.; Schubert, U. S.; Rau, S. A water-soluble copolymer for storage and electron conversion in photocatalytic on-demand hydrogen evolution. *Nat. Comm.* **2026**, *17*, 1141.
(78) Tshepelevitsh, S.; Kütt, A.; Lõkov, M.; Kaljurand, I.; Saame, J.; Heering, A.; Plieger, P. G.; Vianello, R.; Leito, I. On the Basicity of Organic Bases in Different Media. *Eur. J. Org. Chem.* **2019**, *2019*, 6735–6748.
(79) Pellegrin, Y.; Odobel, F. Sacrificial electron donor reagents for solar fuel production. *C. R. Chim.* **2016**, *20*, 283–295.
(80) Cline, E. D.; Adamson, S. E.; Bernhard, S. Homogeneous Catalytic System for Photoinduced Hydrogen Production Utilizing Iridium and Rhodium Complexes. *Inorg. Chem.* **2008**, *47*, 10378–10388.
(81) Smith, P. J.; Mann, C. K. Electrochemical dealkylation of aliphatic amines. *J. Org. Chem.* **1969**, *34*, 1821–1826.
(82) DeLaive, P. J.; Foreman, T. K.; Giannotti, C.; Whitten, D. G. Photoinduced electron transfer reactions of transition-metal complexes with amines. Mechanistic studies of alternate pathways to back electron transfer. *J. Am. Chem. Soc.* **1980**, *102*, 5627–5631.
(83) Whitten, D. G. Photoinduced electron transfer reactions of metal complexes in solution. *Acc. Chem. Res.* **1980**, *13*, 83–90.
(84) Pfeffer, M. G.; Kowacs, T.; Wächtler, M.; Guthmuller, J.; Dietzek, B.; Vos, J. G.; Rau, S. Optimization of Hydrogen-Evolving Photochemical Molecular Devices. *Angew., Chem. Int. Ed.* **2015**, *54*, 6627–6631.
(85) Li, M.; Sakong, S.; Dominguez-Flores, F.; Ma, N.; Groß, A. The Role of Surface Stoichiometry in the Activity of Doped Vanadia-Based Catalysts for the Selective Catalytic Reduction. *Top. Catal.* **2025**, *68*, 1934–1950.
(86) Zedler, L.; Kupfer, S.; Schmidt, H.; Dietzek-Ivanšić, B. Oxidation-state sensitive light-induced dynamics of Ruthenium-4H-Imidazole complexes. *Chem. Eur. J.* **2024**, *30*, e202303079.
(87) Yoshimura, A.; Torieda, H.; Ohno, T. Doublet-Quartet Intersystem Crossing and Electron Transfer of Cobalt(II) Moieties in [LRuIII(L-L)CoIIL]5+ (L = 2, 2′:6′, 2″-Terpyridine and L-L = A Bridging Ligand). *J. Phys. Chem. A* **2004**, *108*, 2149–2154.
(88) Barral, M. C.; Casanova, D.; Herrero, S.; Jiménez-Aparicio, R.; Torres, M. R.; Urbanos, F. A. Tuning the Magnetic Moment of [Ru2(DPhF)3(O2CMe)L]+ Complexes (DPhF=N, N′-Diphenylformamidinate): A Theoretical Explanation of the Axial Ligand Influence. *Chem. Eur. J.* **2010**, *16*, 6203–6211.
(89) Caix, C.; Chardon-Noblat, S.; Deronzier, A.; Moutet, J.-C.; Tingry, S. (Pentamethylcyclopentadienyl)(polypyridyl) rhodium and iridium complexes as electrocatalysts for the reduction of protons to dihydrogen and the hydrogenation of organics. *J. Organomet. Chem.* **1997**, *540*, 105–111.
(90) Henke, W. C.; Lionetti, D.; Moore, W. N. G.; Hopkins, J. A.; Day, V. W.; Blakemore, J. D. Ligand Substituents Govern the Efficiency and Mechanistic Path of Hydrogen Production with [Cp*Rh] Catalysts. *ChemSusChem* **2017**, *10*, 4589–4598.
(91) Quintana, L. M. A.; Johnson, S. I.; Corona, S. L.; Villatoro, W.; Goddard, W. A.; Takase, M. K.; VanderVelde, D. G.; Winkler, J. R.; Gray, H. B.; Blakemore, J. D. Proton–hydride tautomerism in hydrogen evolution catalysis. *Proc. Natl. Acad. Sci. U. S. A.* **2016**, *113*, 6409–6414.
(92) Henke, W. C.; Peng, Y.; Meier, A. A.; Fujita, E.; Grills, D. C.; Polyansky, D. E.; Blakemore, J. D. Mechanistic roles of metal- and ligand-protonated species in hydrogen evolution with [Cp*Rh] complexes. *Proc. Natl. Acad. Sci. U. S. A.* **2023**, *120*, e2217189120.
(93) Johnson, S. I.; Gray, H. B.; Blakemore, J. D.; Goddard, W. A. Role of Ligand Protonation in Dihydrogen Evolution from a Pentamethylcyclopentadienyl Rhodium Catalyst. *Inorg. Chem.* **2017**, *56*, 11375–11386.
(94) Koike, K.; Grills, D. C.; Tamaki, Y.; Fujita, E.; Okubo, K.; Yamazaki, Y.; Saigo, M.; Mukuta, T.; Onda, K.; Ishitani, O. Investigation of excited state, reductive quenching, and intramolec ular electron transfer of Ru(ii)–Re(i) supramolecular photocatalysts for CO2 reduction using time-resolved IR measurements. *Chem. Sci.* **2018**, *9*, 2961–2974.
(95) Yamazaki, Y.; Ohkubo, K.; Saito, D.; Yatsu, T.; Tamaki, Y.; Tanaka, S.; Koike, K.; Onda, K.; Ishitani, O. Kinetics and Mechanism of Intramolecular Electron Transfer in Ru(II)–Re(I) Supramolecular CO2–Reduction Photocatalysts: Effects of Bridging Ligands. *Inorg. Chem.* **2019**, *58*, 11480–11492.
(96) Rivarola, C. R.; Bertolotti, S. G.; Previtali, C. M. Photoreduction of Ru(bpy)32+ by Amines in Aqueous Solution. Kinetics Characterization of a Long-Lived Nonemitting Excited State. *Photochem. Photobiol.* **2006**, *82*, 213.
(97) Kuramochi, Y.; Ishitani, O. Iridium(III) 1-Phenylisoquinoline Complexes as a Photosensitizer for Photocatalytic CO_2 Reduction: A Mixed System with a Re(I) Catalyst and a Supramolecular Photocatalyst. *Inorg. Chem.* **2016**, *55*, 5702–5709.
(98) Tamaki, Y.; Koike, K.; Ishitani, O. Highly efficient, selective, and durable photocatalytic system for CO_2 reduction to formic acid. *Chem. Sci.* **2015**, *6*, 7213–7221.
(99) Kamogawa, K.; Santoro, A.; Cancelliere, A. M.; Shimoda, Y.; Miyata, K.; Onda, K.; Puntoriero, F.; Campagna, S.; Tamaki, Y.; Ishitani, O. Highly Efficient Supramolecular Photocatalysts for CO2 Reduction with Eight Carbon–Carbon Bonds between a Ru(II) Photosensitizer and a Re(I) Catalyst Unit. *ACS Catal.* **2023**, *13*, 9025–9032.
(100) Holleman, A. F.; Nils, W.; Egon, W.; Fischer, G. *Lehrbuch der Anorganischen Chemie*; Walter de Gruyter, **2007**.
(101) Lischka, M.; Groß, A. Hydrogen adsorption on an open metal surface:H_2/Pd(210). *Phys. Rev. B* **2002**, *65*, 075420.
(102) Groß, A.; Scheffler, M. Role of zero-point effects in catalytic reactions involving hydrogen. *J. Vac. Sci. Technol. A* **1997**, *15*, 1624.
(103) Whang, D. R.; Park, S. Y. Rational Design of an Electron-Reservoir PtII Complex for Efficient Photocatalytic Hydrogen Production from Water. *ChemSusChem* **2015**, *8*, 3204–3207.
(104) Escudero, D.; Thiel, W. Exploring the Triplet Excited State Potential Energy Surfaces of a Cyclometalated Pt(II) Complex: Is There Non-Kasha Emissive Behavior? *Inorg. Chem.* **2014**, *53*, 11015–11019.
(105) Kumar, P.; Escudero, D. Computational Protocol to Calculate the Phosphorescence Energy of Pt(II) Complexes: Is the Lowest Triplet Excited State Always Involved in Emission? A Comprehensive Benchmark Study. *Inorg. Chem.* **2021**, *60*, 17230–17240.
(106) Shillito, G. E.; Rau, S.; Kupfer, S. Plugging the 3MC Sink in RuII-Based Photocatalysts. *ChemCatChem* **2023**, *15*, e202201489.
(107) Hernandez-Castillo, D.; Nau, R. E. P.; Schmid, M.; Tschierlei, S.; Rau, S.; Gonzalez, L. Multiple Triplet Metal-Centered Jahn-Teller Isomers Determine Temperature-Dependent Luminescence Lifetimes in $[Ru(bpy)3]^{2+}$. *Angew. Chem., Int. Ed.* **2023**, *62*, e202308803.
(108) Eyring, H.; Polanyi, M. On Simple Gas Reactions. *Z. Phys. Chem.* **2013**, *227*, 1221.

https://doi.org/10.1021/acscatal.6c03235
ACS Catal. XXXX, XXX, XXX–XXX

(109) Evans, M. G.; Polanyi, M. Some applications of the transition state method to the calculation of reaction velocities, especially in solution. *Trans. Faraday Soc.* **1935**, *31*, 875.
(110) Eyring, H. The Activated Complex in Chemical Reactions. *J. Chem. Phys.* **1935**, *3*, 107–115.
(111) Eichler, A.; Hafner, J.; Groß, A.; Scheffler, M. Trends in the chemical reactivity of surfaces studied by ab initio quantum-dynamics calculations. *Phys. Rev. B* **1999**, *59*, 13297.
(112) Collison, D.; Mabbs, F. E.; McInnes, E. J. L.; Taylor, K. J.; Welch, A. J.; Yellowlees, L. J. Electrochemical and spectroelectrochemical studies on platinum complexes containing 2, 2'-bipyridine. *J. Chem. Soc.* **1996**, 329–334.
(113) Yang, L.; Wimmer, F. L.; Wimmer, S.; Zhao, J.; Braterman, P. S. Electro- and spectroelectrochemistry of platinum(II) bipyridine complexes and related species. *J. Organomet. Chem.* **1996**, *525*, 1–8.
(114) Mengele, A. K.; Müller, C.; Nauroozi, D.; Kupfer, S.; Dietzek, B.; Rau, S. Molecular Scylla and Charybdis: Maneuvering between pH Sensitivity and Excited-State Localization in Ruthenium Bi(benz)imidazole Complexes. *Inorg. Chem.* **2020**, *59*, 12097–12110.
(115) Müller, C.; Schwab, A.; Randell, N. M.; Kupfer, S.; Dietzek-Ivanšić, B.; Chavarot-Kerlidou, M. A Combined Spectroscopic and Theoretical Study on a Ruthenium Complex Featuring a π-Extended dppz Ligand for Light-Driven Accumulation of Multiple Reducing Equivalents. *Chem. Eur. J.* **2022**, *28*, e202103882.
(116) Schindler, J.; Traber, P.; Zedler, L.; Zhang, Y.; Lefebvre, J.-F.; Kupfer, S.; Gräfe, S.; Demeunynck, M.; Chavarot-Kerlidou, M.; Dietzek, B. Photophysics of a Ruthenium Complex with a π-Extended Dipyridophenazine Ligand for DNA Quadruplex Labeling. *J. Phys. Chem. A* **2018**, *122*, 6558–6569.
(117) Zedler, L.; Mengele, A. K.; Ziems, K. M.; Zhang, Y.; Wächtler, M.; Gräfe, S.; Pascher, T.; Rau, S.; Kupfer, S.; Dietzek, B. Unraveling the Light-Activated Reaction Mechanism in a Catalytically Competent Key Intermediate of a Multifunctional Molecular Catalyst for Artificial Photosynthesis. *Angew. Chem., Int. Ed.* **2019**, *58*, 13140–13148.
(118) Barker, G. C.; Sammon, D. C. Kinetics of Proton-transfer Reactions. *Nature* **1967**, *213*, 65–66.
(119) Kornyshev, A. A.; Kuznetsov, A. M.; Spohr, E.; Ulstrup, J. Kinetics of Proton Transport in Water. *J. Phys. Chem. B* **2003**, *107*, 3351–3366.
(120) Montgomery, C. L.; Amtawong, J.; Jordan, A. M.; Kurtz, D. A.; Dempsey, J. L. Proton transfer kinetics of transition metal hydride complexes and implications for fuel-forming reactions. *Chem. Soc. Rev.* **2023**, *52*, 7137–7169.
(121) Lämmle, M.; Volk, S.; Klinkerman, M.; Müßler, M.; Mengele, A. K.; Rau, S. Efficient Access of Phenyl-Spaced 5, 5'-Bridged Dinuclear Ruthenium Metal Complexes and the Effect of Dynamic Ligand Exchange on Catalysis. *Photochem* **2022**, *2*, 831–848.
(122) Yamauchi, K.; Masaoka, S.; Sakai, K. Stability of Pt(ii)-based H2-evolving catalysts against H2 in aqueous solution. *Dalton Trans.* **2011**, *40*, 12447.
(123) Ozawa, H.; Aki Haga, M.; Sakai, K. A Photo-Hydrogen-Evolving Molecular Device Driving Visible-Light-Induced EDTA-Reduction of Water into Molecular Hydrogen. *J. Am. Chem. Soc.* **2006**, *128*, 4926–4927.
(124) Sakai, K.; Ozawa, H. Homogeneous catalysis of platinum(II) complexes in photochemical hydrogen production from water. *Coord. Chem. Rev.* **2007**, *251*, 2753–2766.
(125) Lei, P.; Hedlund, M.; Lomoth, R.; Rensmo, H.; Johansson, O.; Hammarström, L. *J. Am. Chem. Soc.* **2007**, *130*, 26–27.

https://doi.org/10.1021/acscatal.6c03235
ACS Catal. XXXX, XXX, XXX–XXX